An Intrinsically Stretchable Nanowire Photodetector with a Fully Embedded Structure

*Chaoyi Yan, Jiangxin Wang, Xu Wang, Wenbin Kang, Mengqi Cui, Ce Yao Foo, and Pooi See Lee**

Stretchable optoelectronics, a form of electronics that can be bended, twisted, folded and stretched, hold the promise to open up unprecedented applications, which are unreachable with existing rigid technology, such as implantable biomedical devices, wearable electronics, smart clothes, and sensory skin for robotic system.[1] Several types of stretchable optoelectronic devices have been successfully demonstrated, including stretchable light-emitting diodes (LEDs),[2–6] stretchable photodetectors,[7–9] stretchable solar cells,[10–12] etc. Photodetectors are a type of electronic device for sensing light and they have found broad applications in consumer electronics such as digital cameras. State-of-the-art technologies employ single-crystal silicon devices on rigid planar substrates.[9] It would be of great interest to make those photodetectors stretchable for innovative applications. For example, stretchable photodetectors could be implanted on human eyes so that one can take digital images by simply blinking. Those implantable photodetectors can also help blind people to regain their visual senses. Compared with existing photodetectors integrated on planar circuit boards, the soft and stretchable devices can deform and comply to surfaces such as the hemispherical lens of human eye and enable new functionalities such as wider field of view, lower aberrations and tunable focal lengths.[8,9,13] Recently, stretchable photodetectors based on single-crystal silicon were fabricated using compressible interconnects, and the devices can be mounted onto an eye-ball lens to improve the imaging capability.[8,9] Herein we present another strategy for fabricating highly-stretchable photodetectors based on nanowire elastic conductors. The photodetectors employ an intrinsically stretchable device structure with both electrodes and detection channels fully embedded in an elastomer matrix and exhibit an excellent stretchability up to 100%.

Imparting stretchability to originally rigid devices can be achieved by proper material and structural designs.[1] Stretchable materials based on elastomers loaded with conductive fillers (such as Ag nanoparticles, carbon nanotubes) have been reported.[3,14–16] Designing stretchable structures is a more commonly employed strategy. For example, metallic films directly deposited on elastomer substrates via evaporation,[17] printing[18,19] or implantation[20] were found to be stretchable. Buckled and serpentine structures of metal[9,21] and graphene[4,22] conducting materials were also designed to achieve desired stretchability. Especially, percolating nanowire and nanotube networks have been shown to be promising candidates for stretchable electronics.[5,14,23–25] The interconnected nanowires within the percolating network can effectively accommodate strain and show fairly good tolerance to stretching before they rupture into patches. To date, several groups have reported the fabrication of stretchable carbon nanotube (CNT) or nanowire networks,[5,14,23–25] however, most of them focused on the demonstration of stretchable electrodes only, and very limited work on the assembly of different functional nanowire components into complete devices can be found. Especially, no studies on stretchable nanowire photodetectors have been reported. In this work, we introduce a lithographic filtration method to fabricate stretchable photodetectors based on embedded nanowires. The method is fast and effective for the fabrication of uniform nanowire films, and it also allows facile integration of multiple patterned nanowire layers for the construction of complex device structures, which is a key advantage over existing "casting" method.

Illustrations of the lithographic filtration method are shown in **Figure 1**a. Different functional components can be integrated into devices based on this method. Two sets of filtration masks for Ag nanowire electrodes and ZnO nanowire channel were prepared from cured polydimethylsiloxane (PDMS) membrane (thickness 1 mm). The soft polymeric masks have similar roles as those hard ultraviolet (UV) masks used in photolithography: to selectively expose certain areas and obtain desired patterns. The mask for electrodes is first put on top of the polycarbonate (PC) filter membrane. Note that the mask is naturally in close contact with the membrane due to the vacuum suction force and sticky surface of polydimethylsiloxane (PDMS), to prevent the spreading of the nanowire dispersion and make well-defined patterns. Ag nanowire dispersions were filtered to get a uniform percolating nanowire film. The filtration process is fast due to the large pore size (220 nm) and high flow rate (3.36 mL cm^2 min^{-1} psi^{-1} for water) of the PC membrane.[26] The as-obtained nanowire film is quite uniform due to the simultaneous extraction of solvent from the uniformly distributed track-etched pores (Figure S1, Supporting Information). The thickness and hence the resistance of the Ag nanowire film can be controlled by the volume of the nanowire dispersion (with fixed nanowire concentration) added. Then, the first mask is removed and the Ag nanowire film is thoroughly rinsed with ethanol. The second mask for ZnO channel is aligned on top of the Ag electrode patterns, and the ZnO nanowire patterns were filtered analogously. Further deposition of multiple functional layers can be readily achieved to obtain even-more-complex device structures. Note

Dr. C. Y. Yan, J. X. Wang, X. Wang, W. B. Kang, M. Q. Cui, C. Y. Foo, Prof. P. S. Lee
School of Materials Science and Engineering
50 Nanyang Avenue
Nanyang Technological University
Singapore, 639798
E-mail: pslee@ntu.edu.sg

DOI: 10.1002/adma.201304226

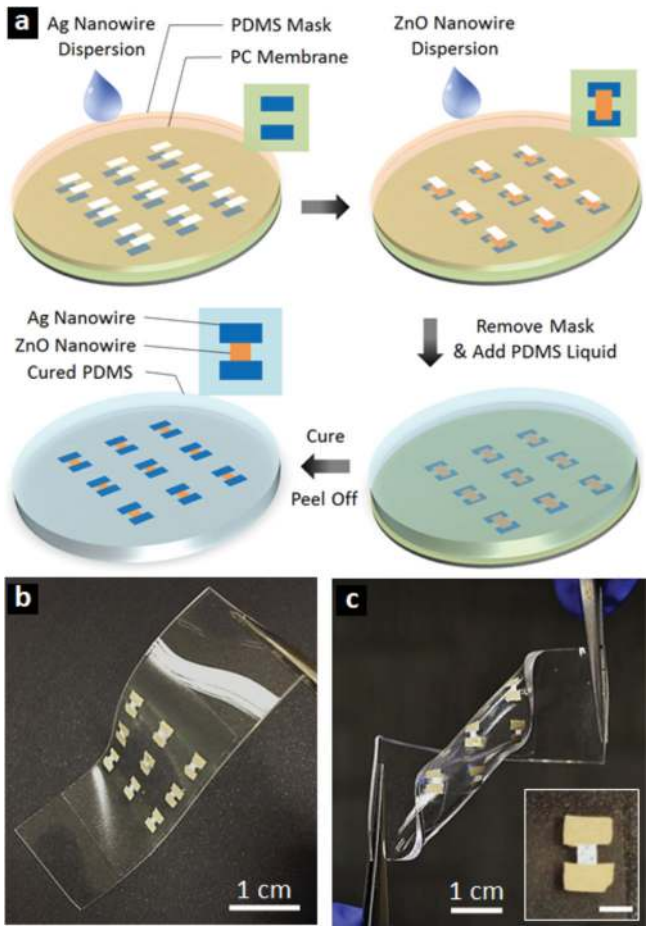

Figure 1. a) Lithographic filtration method for stretchable nanowire photodetector array fabrication. b–c) Digital images of a 3 × 3 photodetector array on PDMS substrate. The inset in (c) is an enlarged view of an individual device with Ag nanowire electrodes and ZnO nanowire channel. The scale bar is 2 mm.

that the size distributions of Ag and ZnO nanowires before and after filtration did not show discernable variation (Figure S2, Supporting Information). Although the diameters of some nanowires are smaller than the pore size of the membrane, it is not easy for the nanowires to go through the pores due to their 1D structure. The filter membrane with Ag and ZnO nanowire patterns is then placed in a glass Petri dish. Liquid PDMS is poured on top of the membrane, degassed for 30 min in a vacuum desiccator, and cured at 60 °C for 2 h. The degassing step is to remove the bubbles and ensure that the liquid PDMS fully penetrates into the porous nanowire film. PDMS has been widely used as transfer printing stamps with molecular-scale resolution,[27,28] and they can efficiently penetrate into the porous nanowire films and produce fully embedded structures (**Figure 2**). The PDMS substrate is peeled off from the filter membrane after solidification with both nanowire electrodes and channels transferred into the PDMS matrix. Examples of the stretchable nanowire photodetector arrays are shown in Figure 1b,c. The inset in Figure 1c is an enlarged view of an individual photodetector made of two symmetric Ag nanowire electrodes and one ZnO nanowire detection channel.

Previously embedded nanowire electrodes have been fabricated via a simple "casting" method.[23,29] The nanowire dispersion was dropped on a flat substrate (glass or polished Si wafer). A layer of percolating nanowire film was formed when the solvent was evaporated. The nanowire film was then infiltrated with elastomer to obtain the stretchable substrate with embedded structure. However, this "casting" method has several drawbacks which limit its application: i) The method is time-consuming as it takes time for the solvent to evaporate. This is especially the case when aqueous solution is used or when the casting process has to be repeated for several times to obtain the nanowire film with desired thickness. ii) Rinsing and washing is needed after nanowire film deposition to remove the surfactants and improve the film conductivity; however, the nanowire film cast on a glass/Si wafer would be easily washed away and damaged. Moreover, the rinsing steps would further prolong the overall processing time. iii) Simply dropping the nanowire dispersion onto glass or Si wafer surface and letting it dry usually leads to a non-uniform nanowire film deposition due to the "coffee-ring" effect.[30,31] Nanowires would preferentially aggregate along the periphery of the liquid droplet, resulting in a thicker deposition along the boundary and limited deposition in the center,[30,31] as has also been observed in our own experiments. Further complex treatments of the substrate or solution are needed to mitigate this problem. iv) The "casting" method has been used to fabricate single-layer nanowire films, such as stretchable conductors, but there are significant difficulties in fabricating multilayer structures using this method, mainly because of the difficulties in making patterns with well-defined shapes and desired layouts through a layer-by-layer (LBL) process. Sequential multilayer deposition is a must for the construction of advanced and future complex device architectures. Herein, we suggest that our lithographic filtration method is a fast process to produce uniform nanowire films and it also allows facile multilayer integration.

The microstructures of the photodetectors are characterized using scanning electron microscopy (SEM). Figure 2a,b shows a comparison of the schematic diagram and the SEM observations. Figure 2b shows that the Ag nanowire electrode is slightly wrinkled, which can be attributed to the residual strain arising from the irreversible sliding of nanowires in the PDMS matrix, as has also been observed previously.[23] The wavelength and amplitude of the wrinkles depend on the nanowire film thickness, the Young's modulus, and the Poisson's ratio, as well as applied strain.[32] The ZnO channel is relatively flat (Figure 2b) due to the larger film thickness (Figure 2d) which makes the nanowire film more stiff.[32] Figure 2c is a cross-sectional view of the electrode-channel overlapping area, with an enlarged view of the overlapped bilayer structure shown in Figure 2d. It can be clearly viewed that the Ag nanowire electrode is on top of the ZnO nanowire channel, as expected from the fabrication processes. The thicknesses of the Ag and ZnO nanowire layers are 15 μm and 35 μm, respectively. Figure 2e is a typical top view of the Ag nanowire electrodes, and Figure 2f is a cross-sectional view of the freshly cut ZnO nanowire channel. It is evident that all the nanowire layers are fully embedded in the PDMS matrix, yielding a structure with all the components (electrodes and detection channels) being intrinsically stretchable.

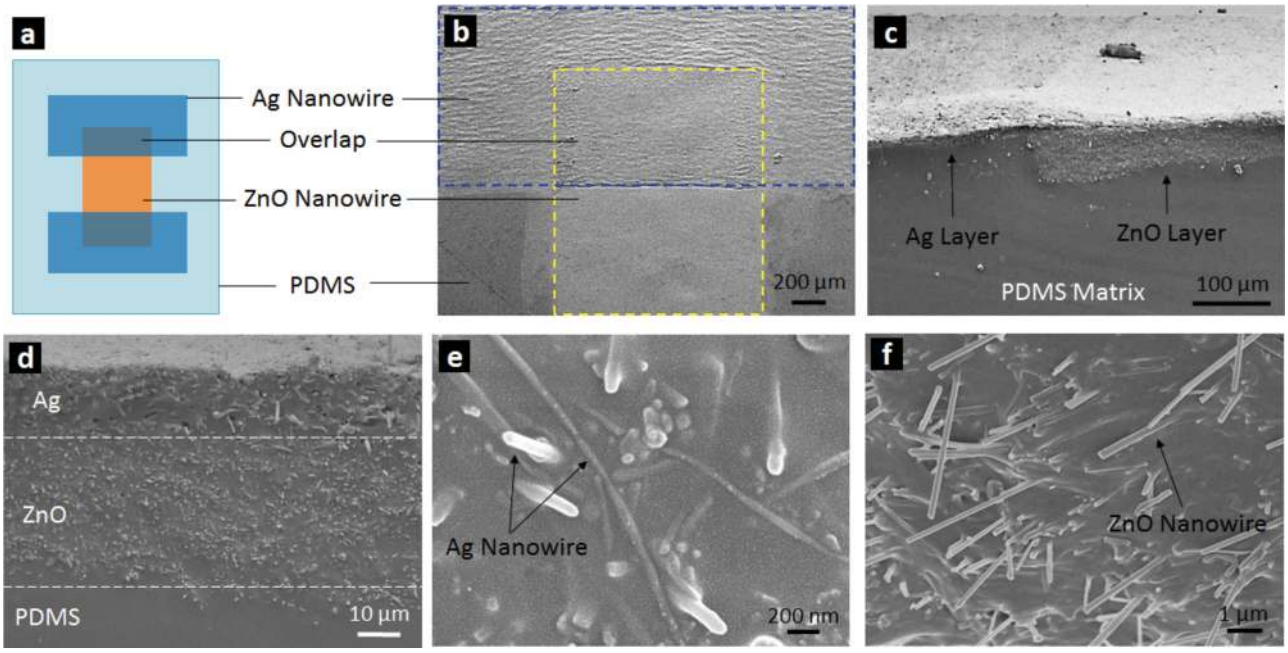

Figure 2. a,b) Comparison of the schematic diagram and SEM image of a photodetector. The planar view of the top electrode region is shown in (b). c) Cross-sectional view of the Ag/ZnO nanowire overlapping area. d) Enlarged view of the overlapped bilayer structure. e) Top view of the Ag nanowire electrodes. f) cross-sectional view of the ZnO nanowire layer embedded in PDMS matrix.

Performances of the photodetectors are shown in **Figure 3**. The photodetector was fixed on a home-built stretching stage to apply desired strain, which is defined as: Strain $= (L - L_0)/L_0$, where L_0 and L are the lengths before and after stretching, respectively. Figure 3b shows the *I*–*V* curves of the photodetector at 0% and 100% strain in the dark and under illumination (365 nm UV light, 0.06 mW cm^{-2}). Good Ohmic conducting behaviors were observed, as expected based on the band alignments of Ag electrodes and ZnO channels where the Schottky barrier is as low as 0.15 eV (Figure S3, Supporting Information). At a fixed voltage of 2 V, the dark versus light currents at 0% and 100% strain are 0.04 versus 8.18 nA and 0.07 vs. 7.83 nA, respectively. Photoresponse behaviors of the device under different strains (from 0% up to 100%) are shown in Figure 3c (see also Figure S4, Supporting Information for the applied signals). The photodetectors were functioning well even at a strain as high as 100%, indicating the excellent stretchability of the devices. Figure 3d is the plot of the ON/OFF ratio versus strain. The ON/OFF ratio decreased from 188 at 0% strain to 116 at 100% strain. A quasi-linear relationship between the ON/OFF ratio and the strain was observed (Figure 3d). The relationship between the ON/OFF ratio and the strain will be discussed later. The response speed is one of the most important characteristics of photodetectors, indicating the switching speed between the ON and the OFF states. Figure 3e,f present curves of the response time and reset time versus strain, respectively. The reset time is defined as the time required to decrease to $1/e$ (37%) of the maximum photocurrent,[33] and consequently, the response time is the time required to increase 63% from the dark current. In Figure 3e, the response time first increases rapidly from 30.3 s (at 0% strain) to 46.5 s (at 20% strain), and then increases slightly from 46.5 s to 51.7 s within 20–100% strain. The reset time displays an increasing trend from 5.8 s at 0% strain to 12.2 s at 100% strain.

To provide further insights into the photoresponse mechanism, the response and reset processes are fitted with corresponding empirical equations (**Figure 4**). The response process can be described by a stretched exponential function:[34,35]

$$I = I_s\left[1 - e^{-(t/\tau)^d}\right] \quad (1)$$

where I_s is the saturation current, τ is the time constant, d is an exponent between 0 and 1 reflecting the response mechanism. Figure 4a is a representative fitting curve for the experimental data at 0% strain. The experimental data were fitted well with Equation 1, with a fitted time constant τ of 32 s and an exponent d of 0.72. The fitted time constants τ for all the response processes (0–100% strain, Figure 4b) followed a similar trend of response time (Figure 3e), which increased rapidly with strain first (0–20% strain) and then increased slightly within 20–100% strain. The plot of fitted exponent d can be found in Figure S5, in the Supporting Information. The reset processes can be described by a second-order exponential decay function:[34,35]

$$I = A_1\exp(-t/\tau_1) + A_2\exp(-t/\tau_2) \quad (2)$$

where A_1 and A_2 are weighing factors, and τ_1 and τ_2 are time constants. Typically we assign $\tau_1 < \tau_2$, so that τ_1 represents the fast component (bulk process) and τ_2 represents the slow component (surface process). Figure 4c shows the fitting of experimental data (0% strain) with Equation 2, with fitted A_1, A_2, τ_1 and τ_2 of 0.69, 0.28, 3.2 s and 27.9 s, respectively. Fitting results from all the reset data showed that for the slow component,

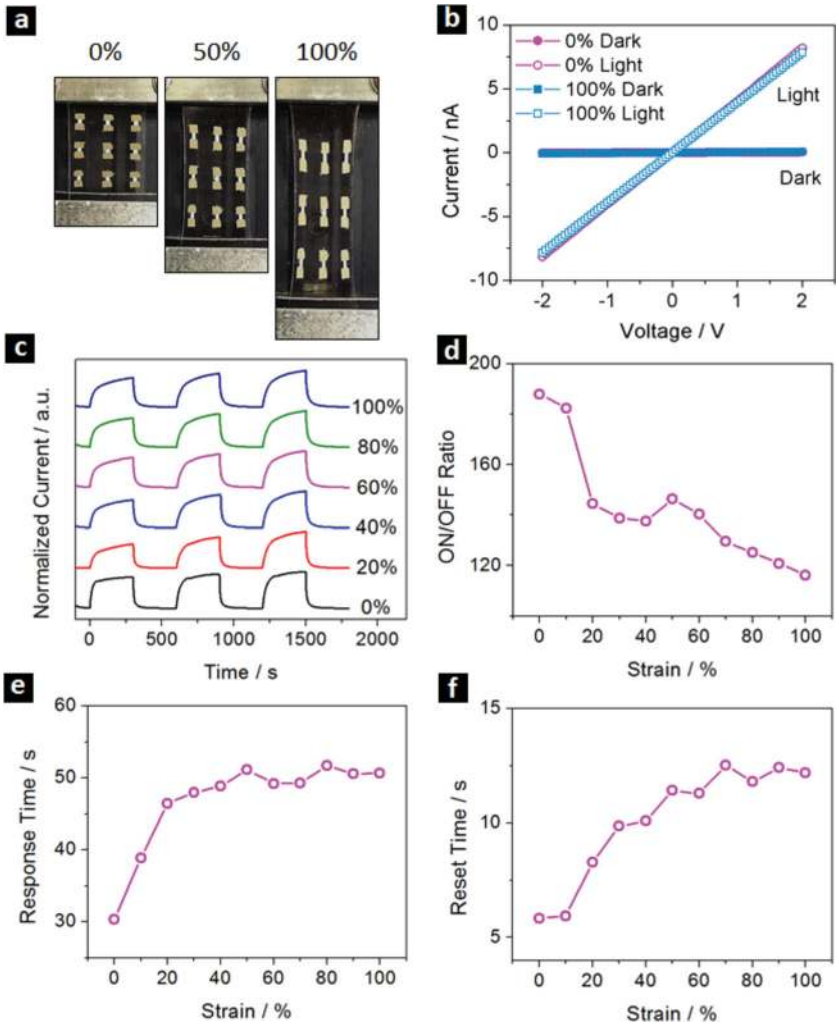

Figure 3. a) Stretching the photodetector to 50% and 100%. b) *I–V* curves of the device at 0% and 100% strain. c) Response behavior of the photodetectors at different strains from 0% to 100%. d–f) Relationships of the ON/OFF ratio, response time and reset time versus strain, respectively.

both the weighing factor (A_2) and time constant (τ_2) increased with strain (Figure 4d), with A_2 increased from 0.29 (at 0% strain) to 0.39 (at 100% strain) and τ_2 increased from 27.8 s (at 0% strain) to 38.6 s (at 100% strain). The fitted time constants for the fast components (τ_1) increase and the corresponding weighing factor (A_1) decreases upon stretching (Figure S5, Supporting Information). The fitting results show that both the response and reset processes become slower when stretched.

The photoresponse behaviors are based on the photoexcitation processes associated with oxygen adsorption and desorption. Oxygen in ambient conditions would adsorb on the nanowire surface, capture free electrons from the nanowire volume via $O_2\,(g) + e^- \rightarrow O_2^-\,(ad)$ and create a surface depletion layer with low conductivity. New electron-hole pairs are generated upon illumination via $h\nu \rightarrow h^+ + e^-$. Holes will be attracted to the negatively charged surface to desorb oxygen via $O_2^-\,(ad) + h^+ \rightarrow O_2\,(g)$ and reduce the depletion layer. The increased electron density together with the reduced depletion layer contributes to the photocurrent increase upon illumination. When the light is turned off, electrons and holes will quickly recombine and lead to significant carrier-density drop. Meanwhile, oxygen will re-adsorb onto the nanowire surface and restore the surface depletion layer.

The photoresponse mechanism for our embedded structures and their variation trend versus strain can be understood based on the elastomer-nanowire surface interactions. Unlike previous photodetectors with nanowires directly exposed in air,[36–39] the ZnO nanowires in our stretchable devices are fully embedded in PDMS matrix (Figure 2f) and surrounded by cross-linked PDMS polymer chains (Figure 4e). Although PDMS is a gas-permeable elastomer, the air solubility is only 15.4 vol% (25 °C, 1 atm),[40] which means that the available oxygen in the nanowire surrounding environments is >6 times lower than that in air. Moreover, the diffusion coefficient of oxygen was reported as 5.2×10^{-6}–3.4×10^{-5} $cm^2\ s^{-1}$ in cross-linked PDMS,[41–44] which is at least 5000 times slower than that in air (1.76×10^{-1} $cm^2\ s^{-1}$).[45] The relationship between photoresponse speed and oxygen levels was systematically studied in previous reports,[46] which showed that both the response and reset processes became slower at reduced oxygen pressures. Meanwhile, unlike the Schottky contact, which dominates the device resistance and responds quickly to incident light, photodetectors with an Ohmic contact usually have a slower photoresponse speed.[33,39] Thus, we expect a relatively slow switching speed for our stretchable photodetectors considering the low oxygen content, slow gas diffusion rate, and Ohmic-type conducting behaviors. The response/reset times were found to be typically in the range of 5–60 s (Figure 3).

Another crucial point is to understand the photodetector performance variation with strain, such as the ON/OFF ratio and switching speed. Since Ag nanowire electrodes exhibit much lower resistances (tens of Ohms) than the ZnO nanowire channel (ca. 10^8 to 10^{10} Ω), they have negligible effects on the photocurrent variations (Figure S6, Supporting Information). Oxygen molecules are adsorbed on part of the nanowire surfaces (due to the limited air solubility ca. 15 vol%) with the rest of the surfaces covered by crosslinked polymer chains (Figure 4e). Upon stretching, the PDMS substrate is laterally compressed and thus the surrounding polymer chains are in more intimate contact with the nanowires (Figure 3a and Figure 4e). This leads to ZnO nanowires having an increased contact area with the polymer chains but a decreased contact area with the air. Part of the oxygen adsorbed on the nanowire surface will be squeezed out upon stretching, which is equivalent to a reduction of the oxygen content in the local surroundings of

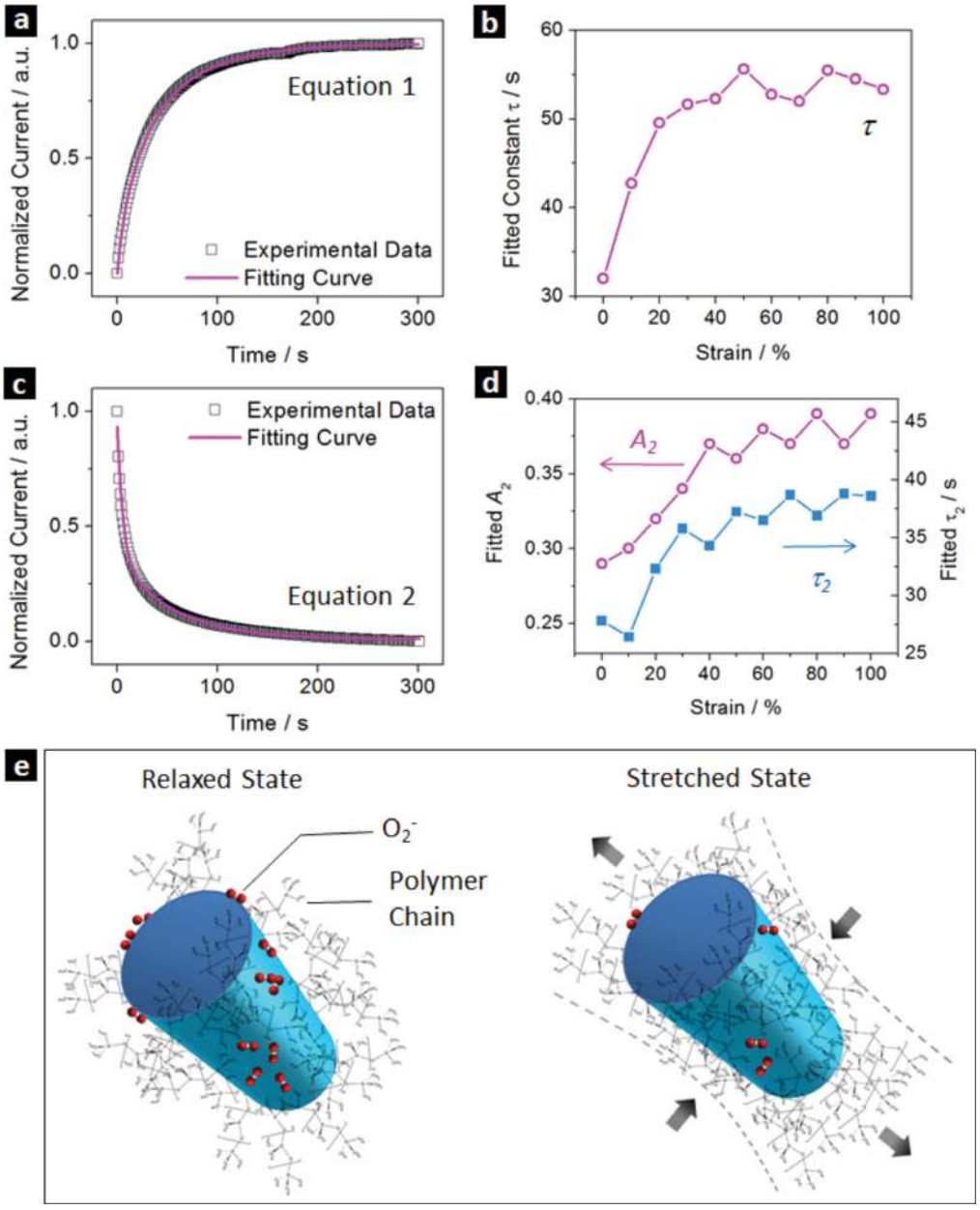

Figure 4. a) Fitting of the response curve (0% strain). b) Fitted τ for the response processes at different strains. c) Fitting of the reset curve (0% strain). d) Fitted values of A_2 and τ_2 for the reset processes at different stains. e) Schematic of the nanowire-polymer chain interactions at relaxed state and stretched state.

the nanowires. Previous extensive studies on nanowire photodetectors have shown that the switching speed decreases with lower oxygen concentration;[36,46–52] thus, slower switching behaviors are expected upon stretching. Meanwhile, the compressed polymer chains may further hinder the oxygen diffusion and the reduced diffusion coefficient will also contribute to the retarded photoresponse speed in stretched states. Briefly, when the photodetectors are stretched, the equivalent oxygen concentration and effective oxygen diffusion coefficient in the nanowire surrounding environment may decrease and lead to slower switching behaviors. This is consistent with our findings: upon stretching, the depletion layer and hence the contact barrier are reduced due to the lower oxygen content. As a result, the current difference (ON/OFF ratio) before and after illumination is lower. The increased response time (Figure 3e) and the fitted time constant (Figure 4b) correspond to slower response processes, due to the longer time it takes to reach adsorption-desorption balance,[46] with a lower oxygen level and slower diffusion rates at stretched states. The larger reset time at higher strain (Figure 3f) is because of the slower oxygen diffusion and re-adsorption processes to restore the surface depletion layer. Especially, the fitting results for the slow components

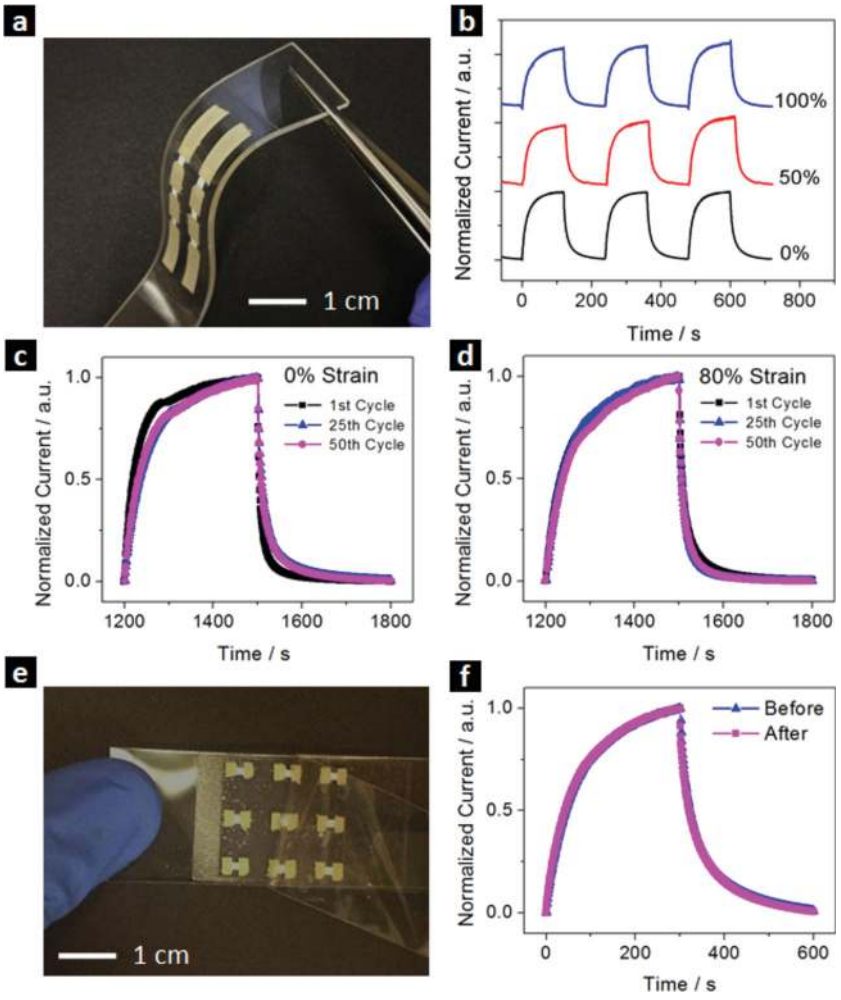

Figure 5. a) Example image and b) switching behaviors of a stretchable device with three photodetectors connected in series. Cycling stability of the photodetectors at: c) 0% strain and d) 80% strain up to 50 cycles. e) Scotch tape testing of the photodetector array and f) corresponding response curves before and after testing (0% strain).

(surface-related) show that the time constant τ_2 became larger upon stretching, and the slow components also increasingly become more dominate (A_2) at higher strains. Fitting results for other parameters and related explanations can be found in Figure S5, Supporting Information.

Our lithographic filtration method allows facile fabrication of complex device structures such as interconnected photodetectors arrays to enable potential multifunctionalities. As a proof-of-concept, we fabricated stretchable devices with three photodetectors connected in series. A photograph of the stretchable photodetector array is shown in **Figure 5**a (see also Figure S7, Supporting Information). Analogous to the isolated photodetectors in Figure 3a, the interconnected photodetectors can be stretched upto 100% and maintain proper functionalities. Typical switching behaviors of the interconnected photodetectors at 0, 50, and 100% strains are shown in Figure 5b. Incorporation of different functional nanowires into the photodetector units to achieve advanced functionalities such as wavelength selectivity[53] can be readily achieved and will be pursued in future studies. The stretchable photodetectors with fully embedded structures possess excellent cycling and mechanical stabilities against repeated stretching, adhesion, or rubbing forces on the surface. The cyclic stretching and Scotch tape testing results are shown in Figure 5c–f. The devices were repeatedly stretched to 80% strain for 1, 25, and 50 cycles, and their corresponding response behaviors were recorded. We set the maximum cycling strain as 80% to ensure that the device could survive the repeated stretching cycles. The first cycle for 0% strain means that the device is freshly made without any stretching (Figure 5c, black curve), so the response curve deviates a little from those after stretching, due to irreversible nanowire sliding and arrangements after stretching.[23] The rest of the response curves remain nearly unchanged for both 0% and 80% strain after 50 cycles, indicating excellent stability against repeated stretching. Another advantage of our fully embedded device structure is that they are mechanically stable against mechanical scratching or adhesive forces. A piece of Scotch tape (Nikko Stationery Tape) was firmly pressed onto the device surface (Figure 5e) and then peeled off. No obvious changes of the device performances were observed before and after the Scotch tape testing (Figure 5f). Unlike those stretchable devices with all components (usually buckled nanostructures) on top of the substrate which are prone to delamination and mechanical damage, our fully embedded device structure, with all components protected inside the rubber matrix, showed significantly improved mechanical stability.

In summary, we present a lithographic filtration method to fabricate stretchable photodetectors with fully embedded structures. Both the electrodes and detection channels are intrinsically stretchable. The devices maintain their functionalities even when stretched up to 100% strain. Detailed analyses showed that when stretched, the ON/OFF ratio decreased and both the response and reset processes became slower, which can be attributed to the nanowire-polymer chain interactions. The stretchable photodetectors also showed excellent cycling and mechanical stabilities, with no obvious performance degradation after 50 repeated stretching cycles and Scotch tape tests. The fabrication method can be readily extended to a wide range of nanowire photodetectors, which may find important applications in future stretchable, wearable, and implantable electronics.

Experimental Section

The ZnO nanowires were grown via chemical vapor deposition (CVD) method as described previously.[54] The as-obtained ZnO nanowires on Si substrates were put in ethanol and sonicated for 30 s to prepare the

nanowire dispersion (typically with a concentration of 0.05 mg mL^{-1}). Commercially available Ag nanowires dispersed in ethanol (2 mg mL^{-1}) were used as received. The lengths of the Ag nanowires were 20–100 μm and diameters were within 40–100 nm.

The PDMS (Sylgard 184, Dow Corning) mask was prepared by curing a degassed mixture of a base and a curer (weight ratio 10:1) at 60 °C for 2 h. Then, the solidified membrane (thickness ca. 1 mm) was cut with a graver to obtain the desired patterns. Two sets of masks were prepared for Ag nanowire electrodes and ZnO nanowire channels, respectively. The PDMS hard masks were put on top of PC filter membranes (Millipore GTTP, pore size 220 nm) to filter the nanowire patterns. The Ag nanowire patterns were filtered first followed by the ZnO nanowire patterns. The filter membrane with the nanowire patterns was then put in a glass Petri dish. Mixed PDMS base and curer (weight ratio 10:1) was poured into the Petri dish, degassed for 30 min in a vacuum desiccator and then cured at 60 °C for 2 h. After curing, the solid PDMS membrane was peeled off from the membrane and the nanowire patterns were transferred to the PDMS substrate. The devices were used for testing without any further treatments.

The morphologies of the nanowires and devices were characterized using field-emission SEM (FE-SEM) (JSM 7600F). The photoresponse behaviors of the devices were characterized using a Keithley analyzer with a portable UV lamp as the light source (365 nm). The device was fixed on a home-made stretching stage to apply strain. All the measurements were performed at room temperature in ambient conditions.

Supporting Information

Supporting Information is available from the Wiley Online Library or from the author.

Acknowledgements

This work was supported in part by the Singapore National Research Foundation (CREATE Programme of Nanomaterials for Energy and Water Management). The authors thank M. F. Lin and X. W. Yan for their technical support and insightful discussions.

Received: August 13, 2013
Revised: September 15, 2013
Published online: November 20, 2013

[1] J. A. Rogers, T. Someya, Y. G. Huang, *Science* **2010**, *327*, 1603.
[2] R. H. Kim, D. H. Kim, J. L. Xiao, B. H. Kim, S. I. Park, B. Panilaitis, R. Ghaffari, J. M. Yao, M. Li, Z. J. Liu, V. Malyarchuk, D. G. Kim, A. P. Le, R. G. Nuzzo, D. L. Kaplan, F. G. Omenetto, Y. G. Huang, Z. Kang, J. A. Rogers, *Nat. Mater.* **2010**, *9*, 929.
[3] T. Sekitani, H. Nakajima, H. Maeda, T. Fukushima, T. Aida, K. Hata, T. Someya, *Nat. Mater.* **2009**, *8*, 494.
[4] R. H. Kim, M. H. Bae, D. G. Kim, H. Y. Cheng, B. H. Kim, D. H. Kim, M. Li, J. Wu, F. Du, H. S. Kim, S. Kim, D. Estrada, S. W. Hong, Y. G. Huang, E. Pop, J. A. Rogers, *Nano Lett.* **2011**, *11*, 3881.
[5] Z. B. Yu, X. F. Niu, Z. T. Liu, Q. B. Pei, *Adv. Mater.* **2011**, *23*, 3989.
[6] H. L. Filiatrault, G. C. Porteous, R. S. Carmichael, G. J. E. Davidson, T. B. Carmichael, *Adv. Mater.* **2012**, *24*, 2673.
[7] P. Bartu, R. Koeppe, N. Arnold, A. Neulinger, L. Fallon, S. Bauer, *J. Appl. Phys.* **2010**, *107*, 123101.
[8] Y. M. Song, Y. Xie, V. Malyarchuk, J. Xiao, I. Jung, K.-J. Choi, Z. Liu, H. Park, C. Lu, R.-H. Kim, R. Li, K. B. Crozier, Y. Huang, J. A. Rogers, *Nature* **2013**, *497*, 95.
[9] H. C. Ko, M. P. Stoykovich, J. Z. Song, V. Malyarchuk, W. M. Choi, C. J. Yu, J. B. Geddes, J. L. Xiao, S. D. Wang, Y. G. Huang, J. A. Rogers, *Nature* **2008**, *454*, 748.
[10] D. J. Lipomi, B. C. K. Tee, M. Vosgueritchian, Z. N. Bao, *Adv. Mater.* **2011**, *23*, 1771.
[11] M. Kaltenbrunner, M. S. White, E. D. Glowacki, T. Sekitani, T. Someya, N. S. Sariciftci, S. Bauer, *Nat. Commun.* **2012**, *3*, 770.
[12] J. Lee, J. A. Wu, M. X. Shi, J. Yoon, S. I. Park, M. Li, Z. J. Liu, Y. G. Huang, J. A. Rogers, *Adv. Mater.* **2011**, *23*, 986.
[13] F. Carpi, G. Frediani, S. Turco, D. De Rossi, *Adv. Funct. Mater.* **2011**, *21*, 4152.
[14] T. Sekitani, Y. Noguchi, K. Hata, T. Fukushima, T. Aida, T. Someya, *Science* **2008**, *321*, 1468.
[15] M. Park, J. Im, M. Shin, Y. Min, J. Park, H. Cho, S. Park, M. B. Shim, S. Jeon, D. Y. Chung, J. Bae, U. Jeong, K. Kim, *Nat. Nanotechnol.* **2012**, *7*, 803.
[16] K. Y. Chun, Y. Oh, J. Rho, J. H. Ahn, Y. J. Kim, H. R. Choi, S. Baik, *Nat. Nanotechnol.* **2010**, *5*, 853.
[17] S. P. Lacour, S. Wagner, Z. Y. Huang, Z. Suo, *Appl. Phys. Lett.* **2003**, *82*, 2404.
[18] A. P. Robinson, I. Minev, I. M. Graz, S. P. Lacour, *Langmuir* **2011**, *27*, 4279.
[19] S. Chung, J. Lee, H. Song, S. Kim, J. Jeong, Y. Hong, *Appl. Phys. Lett.* **2011**, *98*, 153110.
[20] G. Corbelli, C. Ghisleri, M. Marelli, P. Milani, L. Ravagnan, *Adv. Mater.* **2011**, *23*, 4504.
[21] S. Xu, Y. H. Zhang, J. Cho, J. Lee, X. Huang, L. Jia, J. A. Fan, Y. W. Su, J. Su, H. G. Zhang, H. Y. Cheng, B. W. Lu, C. J. Yu, C. Chuang, T. I. Kim, T. Song, K. Shigeta, S. Kang, C. Dagdeviren, I. Petrov, P. V. Braun, Y. G. Huang, U. Paik, J. A. Rogers, *Nat. Commun.* **2013**, *4*, 1543.
[22] K. S. Kim, Y. Zhao, H. Jang, S. Y. Lee, J. M. Kim, K. S. Kim, J. H. Ahn, P. Kim, J. Y. Choi, B. H. Hong, *Nature* **2009**, *457*, 706.
[23] F. Xu, Y. Zhu, *Adv. Mater.* **2012**, *24*, 5117.
[24] P. Lee, J. Lee, H. Lee, J. Yeo, S. Hong, K. H. Nam, D. Lee, S. S. Lee, S. H. Ko, *Adv. Mater.* **2012**, *24*, 3326.
[25] D. J. Lipomi, M. Vosgueritchian, B. C. K. Tee, S. L. Hellstrom, J. A. Lee, C. H. Fox, Z. N. Bao, *Nat. Nanotechnol.* **2011**, *6*, 788.
[26] Millipore PC filter membrane GTTP04700, http://www.millipore.com; accessed, August 2013.
[27] M. A. Meitl, Z. T. Zhu, V. Kumar, K. J. Lee, X. Feng, Y. Y. Huang, I. Adesida, R. G. Nuzzo, J. A. Rogers, *Nat. Mater.* **2006**, *5*, 33.
[28] F. Hua, Y. G. Sun, A. Gaur, M. A. Meitl, L. Bilhaut, L. Rotkina, J. F. Wang, P. Geil, M. Shim, J. A. Rogers, A. Shim, *Nano Lett.* **2004**, *4*, 2467.
[29] S. Yun, X. F. Niu, Z. B. Yu, W. L. Hu, P. Brochu, Q. B. Pei, *Adv. Mater.* **2012**, *24*, 1321.
[30] P. J. Yunker, T. Still, M. A. Lohr, A. G. Yodh, *Nature* **2011**, *476*, 308.
[31] M. Layani, M. Gruchko, O. Milo, I. Balberg, D. Azulay, S. Magdassi, *ACS Nano* **2009**, *3*, 3537.
[32] C. J. Yu, C. Masarapu, J. P. Rong, B. Q. Wei, H. Q. Jiang, *Adv. Mater.* **2009**, *21*, 4793.
[33] J. Zhou, Y. D. Gu, Y. F. Hu, W. J. Mai, P. H. Yeh, G. Bao, A. K. Sood, D. L. Polla, Z. L. Wang, *Appl. Phys. Lett.* **2009**, *94*, 191103.
[34] J. Reemts, A. Kittel, *J. Appl. Phys.* **2007**, *101*, 013709.
[35] R. S. Aga, D. Jowhar, A. Ueda, Z. Pan, W. E. Collins, R. Mu, K. D. Singer, J. Shen, *Appl. Phys. Lett.* **2007**, *91*, 232108.
[36] C. Soci, A. Zhang, B. Xiang, S. A. Dayeh, D. P. R. Aplin, J. Park, X. Y. Bao, Y. H. Lo, D. Wang, *Nano Lett.* **2007**, *7*, 1003.
[37] C. Y. Yan, N. Singh, P. S. Lee, *Appl. Phys. Lett.* **2010**, *96*, 053108.
[38] L. Li, P. S. Lee, C. Y. Yan, T. Y. Zhai, X. S. Fang, M. Y. Liao, Y. Koide, Y. Bando, D. Golberg, *Adv. Mater.* **2010**, *22*, 5145.
[39] C. Y. Yan, N. Singh, H. Cai, C. L. Gan, P. S. Lee, *ACS Appl. Mater. Interfaces* **2010**, *2*, 1794.
[40] Y. Kamiya, Y. Naito, T. Hirose, K. Mizoguchi, *J. Polym. Sci., Part B: Polym. Phys.* **1990**, *28*, 1297.
[41] T. C. Merkel, V. I. Bondar, K. Nagai, B. D. Freeman, I. Pinnau, *J. Polym. Sci., Part B: Polym. Phys.* **2000**, *38*, 415.

[42] M. E. Cox, B. Dunn, *J. Polym. Sci., Part A: Polym. Chem.* **1986**, *24*, 621.
[43] I. De Bo, H. Van Langenhove, P. Pruuost, J. De Neve, J. Pieters, I. F. J. Vankelecom, E. Dick, *J. Membrane Sci.* **2003**, *215*, 303.
[44] A. Zanzotto, N. Szita, P. Boccazzi, P. Lessard, A. J. Sinskey, K. F. Jensen, *Biotechnol. Bioeng.* **2004**, *87*, 243.
[45] E. L. Cussler, *Diffusion: Mass Transfer in Fluid Systems, 2nd ed.* Cambridge University Press, New York **1997**.
[46] Q. H. Li, T. Gao, Y. G. Wang, T. H. Wang, *Appl. Phys. Lett.* **2005**, *86*, 123117.
[47] Q. Wan, E. Dattoli, W. Lu, *Small* **2008**, *4*, 451.
[48] Y. Liu, Z. Y. Zhang, H. L. Xu, L. H. Zhang, Z. X. Wang, W. L. Li, L. Ding, Y. F. Hu, M. Gao, Q. Li, L. M. Peng, *J. Phys. Chem. C* **2009**, *113*, 16796.
[49] Q. H. Li, Q. Wan, Y. X. Liang, T. H. Wang, *Appl. Phys. Lett.* **2004**, *84*, 4556.
[50] D. S. Wang, C. H. Hao, W. Zheng, Q. Peng, T. H. Wang, Z. M. Liao, D. P. Yu, Y. D. Li, *Adv. Mater.* **2008**, *20*, 2628.
[51] H. Kind, H. Q. Yan, B. Messer, M. Law, P. D. Yang, *Adv. Mater.* **2002**, *14*, 158.
[52] P. Feng, J. Y. Zhang, Q. Wan, T. H. Wang, *J. Appl. Phys.* **2007**, *102*, 074309.
[53] Y.-J. Yoon, K.-S. Park, J.-H. Heo, J.-G. Park, S. Nahm, K. J. Choi, *J. Mater. Chem.* **2010**, *20*, 2386.
[54] M. H. Huang, Y. Y. Wu, H. Feick, N. Tran, E. Weber, P. D. Yang, *Adv. Mater.* **2001**, *13*, 113.